

Study of wave chaos in a randomly-inhomogeneous oceanic acoustic waveguide: spectral analysis of the finite-range evolution operator

D.V. Makarov,^{1,*} L.E. Kon'kov,¹ M.Yu. Uleysky,¹ and P.S. Petrov^{1,2}

¹*V.I. Il'ichev Pacific Oceanological Institute
of the Far-Eastern Branch of the Russian Academy of Sciences,
43 Baltiyskaya St., 690041, Vladivostok, Russia*

²*Far-East Federal University,
8 Sukhanova St., 690950, Vladivostok, Russia*

The problem of sound propagation in an oceanic waveguide is considered. Scattering on random inhomogeneity of the waveguide leads to wave chaos. Chaos reveals itself in spectral properties of the finite-range evolution operator (FREO). FREO describes transformation of a wavefield in course of propagation along a finite segment of a waveguide. We study transition to chaos by tracking variations in spectral statistics with increasing length of the segment. Analysis of the FREO is accompanied with ray calculations using the one-step Poincaré map which is the classical counterpart of the FREO. Underwater sound channel in the Sea of Japan is taken for an example. Several methods of spectral analysis are utilized. In particular, we approximate level spacing statistics by means of the Berry-Robnik and Brody distributions, explore the spectrum using the procedure elaborated by A. Relano with coworkers (Relano et al, Phys. Rev. Lett., 2002; Relano, Phys. Rev. Lett., 2008), and analyze modal expansions of the eigenfunctions. We show that the analysis of FREO eigenfunctions is more informative than the analysis of eigenvalue statistics. It is found that near-axial sound propagation in the Sea of Japan preserves stability even over distances of hundreds kilometers. This phenomenon is associated with the presence of a shearless torus in the classical phase space. Increasing of acoustic wavelength degrades scattering, resulting in recovery of localization near periodic orbits of the one-step Poincaré map. Relying upon the formal analogy between wave and quantum chaos, we suggest that the concept of FREO, supported by classical calculations via the one-step Poincaré map, can be efficiently applied for studying chaos-induced decoherence in quantum systems.

PACS numbers: 05.45.Mt, 43.30.Cq, 03.65.Yz, 05.45.Ac, 43.30.Ft

I. INTRODUCTION

Sound speed in the deep ocean typically has a minimum at some depth. This results in formation of a refractive waveguide, the so-called underwater sound channel, which prevents sound waves from contact with the absorbing bottom. As sound absorption within water column is fairly weak, an underwater sound channel enables sound propagation over distances of thousands kilometers. The largest distance had been achieved using explosive charges in the seminal experiment on sound transmission from Perth to Bermuda in 1960 [1, 2].

It is realized that small sound-speed variations induced by oceanic internal waves lead to Lyapunov instability and chaos of sound rays. In the mathematical sense, ray chaos is an analogue of classical chaos in Hamiltonian systems. Indeed, ray motion in a waveguide is equivalent to motion of a point particle in a potential well, and sound-speed variations along a waveguide play the role of a nonstationary perturbation. Reciprocal Lyapunov exponent for chaotic rays typically is of about several tens kilometers [3], therefore, the problem of ray chaos is mainly important for long-range sound propagation. During the last two decades ray chaos in ocean

acoustics was an object of intense research, both theoretical and experimental [4–8]. Considerable attention was paid to wave chaos [3, 9–14]. The term wave chaos relates to wavefield manifestations of ray chaos. It was found that interference makes wave refraction more regular than it is anticipated from ray modeling, albeit influence of ray chaos persists even for very low sound frequencies [15]. This problem becomes especially important due to the growing interest to hydroacoustical tomography, i. e. monitoring of environment using sound signals. The classical scheme of tomography developed by Munk and Wunsch [16] is based on computation of eigenrays connecting the source and the receiver. It was shown in [17] that ray chaos leads to exponential proliferation of eigenrays with increasing distance. As a result, the inverse problem becomes ill-posed, impeding environment reconstruction. However, wave-based corrections “stabilize” wave refraction, i. e. the standard semiclassical approximation typically overestimates ray chaos. Thus, one needs either an improved version of the semiclassical approximation for proper computation of eigenrays, or some approach for making implications about eigenray stability relying upon wave modeling, whereby a priori taking into account the wave-based suppression of ray chaos.

Theory of ray and wave chaos extensively exploits methods borrowed from the theory of Hamiltonian dynamical systems [3, 18]. In particular, ray motion is

* makarov@poi.dvo.ru

often studied by means of the phase space representation. This provides the clear geometric interpretation of ray dynamics for toy models of deterministic range-periodic waveguides. For instance, one can easily separate domains of initial conditions corresponding to stable and chaotic rays from each other. However, realistic underwater sound channels are not range-periodic, and their range inhomogeneity should be rather described as a stochastic process. On the other hand, statistical methods [19, 20] are implicitly based on the assumption of ergodic chaos and ignore the existence of phase space domains of finite-range stability [21, 22]. Therefore, it is reasonable to elaborate some theoretical approach combining advantages of statistical and deterministic methods. Recently it had been shown that a bridge between the deterministic and statistical descriptions of wave propagation in random media can be built up by introducing the finite-range evolution operator (hereafter FREO) [14, 23]. FREO acts as a propagator determining wavefield transformation between two vertical sections of a waveguide. Spectral analysis of the FREO in terms of the random matrix theory allows one to estimate contribution of ray chaos to wave dynamics and track transition to chaos with increasing distance between the sections. A somewhat different approach had been offered in [24]. These approaches allow one to generalize the well-developed spectral theory of quantum chaos (see, for instance, [25]) on one-way wave propagation in random media. On the other hand, concept of the FREO can serve as a promising method for studying chaos-induced decoherence in randomly-driven quantum systems [26].

In the present paper we study spectral statistics of the FREO for the Sea of Japan. Attention is concentrated on the track connecting the Gamov peninsula and Kitayama bank. The length of the track is about 350 km. Our interest to this waveguide is motivated by results of the experiment conducted there in 2006 [27], indicating on high stability of near-axial propagation. Similar behavior was observed in a earlier experiment with a slightly different propagation track [28]. It should be noted that stability of near-axial propagation is atypical for the deep ocean [3, 14].

The paper is organized as follows. The next section represents basic equations describing long-range sound propagation in the ocean. In Section III, we describe the waveguide used in the paper. Section IV contains description of the FREO and methods of its analysis. Section V is devoted to the classical counterpart of the FREO, namely the one-step Poincaré map. In Section VI, we perform statistical analysis of the FREO for the underwater sound channel in the Sea of Japan. In Conclusion we summarize and discuss the results obtained.

II. GENERAL EQUATIONS

Ocean is a layered media, and its horizontal variability is much weaker than vertical one. This allows one

to reduce the initial three-dimensional problem of wave propagation in an underwater sound channel to a two-dimensional one by assuming cylindrical symmetry and neglecting azimuthal coupling. Sound refraction is governed by spatial variability of sound speed

$$c(z, r) = c_0 + \Delta c(z) + \delta c(z, r), \quad (1)$$

where z is depth, r is range coordinate, c_0 is a reference sound speed. Sound-speed variations obey the double inequality

$$|\delta c|_{\max} \ll |\Delta c|_{\max} \ll c_0. \quad (2)$$

Left inequality implies that the range-dependent term can be treated as a weak perturbation of the background sound-speed profile. This term is mainly contributed from oceanic internal waves. Right inequality means that variations of the refractive index are weak, and only those waves which propagate with small angles with respect to the horizontal plane can avoid contact with the absorbing ocean bottom. Thus, one can invoke the small-angle approximation, in which an acoustic wavefield is governed by the standard parabolic equation

$$\frac{i}{k_0} \frac{\partial \Phi}{\partial r} = -\frac{1}{2k_0^2} \frac{\partial^2 \Phi}{\partial z^2} + [U(z) + \varepsilon V(z, r)] \Phi, \quad (3)$$

where wave function Φ is linked to acoustic pressure u by means of the formula $u = \Phi \exp(ik_0 r) / \sqrt{r}$. Here the denominator \sqrt{r} responds for the cylindrical spreading of sound. Quantity k_0 is the reference wavenumber related to sound frequency f as $k_0 = 2\pi f / c_0$. Functions $U(z)$ and $V(z, r)$ are determined by spatial sound-speed variations. In the the small-angle approximation they can be expressed as

$$U(z) = \frac{\Delta c(z)}{c_0}, \quad V(z, r) = \frac{\delta c(z, r)}{c_0}. \quad (4)$$

According to (2), $|V|_{\max} \ll |U|_{\max}$, that is, function $V(z, r)$ can be treated as a small perturbation. One can easily see that the replacement

$$k_0^{-1} \rightarrow \hbar, \quad r \rightarrow t \quad (5)$$

transforms the parabolic equation (3) into the Schrödinger equation for a particle with unit mass. This circumstance enables study of wave propagation using the approaches developed in quantum mechanics. In this relationship, function $U(z)$ serves as an unperturbed potential. As r is a timelike variable, $V(z, r)$ plays the role of a nonstationary perturbation.

In the short-wavelength limit $k_0 \rightarrow \infty$, solution of the parabolic equation (3) can be expressed as a sum of rays whose trajectories are governed by the Hamiltonian

$$H = \frac{p^2}{2} + U(z) + V(z, r), \quad (6)$$

where $p = \tan \chi$, χ is ray grazing angle (i. e. angle with respect to the horizontal plane). The respective Hamiltonian equations read

$$\frac{dz}{dr} = \frac{\partial H}{\partial p} = p, \quad \frac{dp}{dr} = -\frac{\partial H}{\partial z} = -\frac{\partial U}{\partial z} - \frac{\partial V}{\partial z}. \quad (7)$$

Owing to the analogy with classical mechanics, p is referred to as *ray momentum*.

III. MODEL OF A WAVEGUIDE

A. Background sound-speed profile

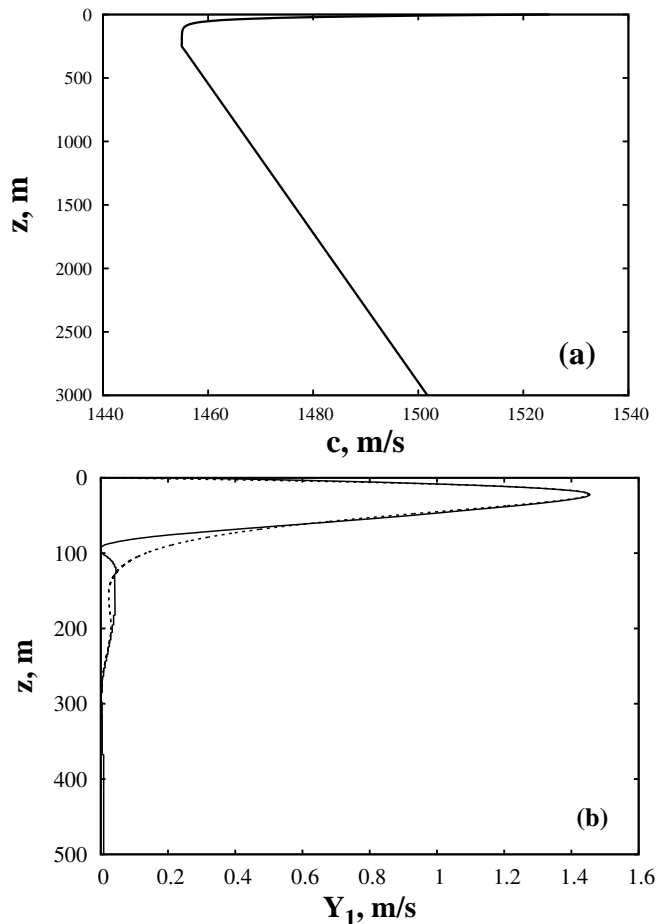


FIG. 1. (a) Unperturbed sound-speed profile, (b) the first empirical orthogonal function of the sound-speed perturbation (solid) and its smoothed approximation (dotted).

Model of the underwater sound channel in the Sea of Japan was elaborated using the hydrological data from the database [29]. Function $U(z)$ corresponding to the background sound-speed profile was approximated by the expression

$$U(z) = \begin{cases} U_1(z), & z \leq z_0, \\ U_2(z), & z > z_0. \end{cases} \quad (8)$$

where

$$\begin{aligned} U_1(z) &= \frac{c_1}{c_0} e^{-z/z_1}, \\ U_2(z) &= \frac{c_1}{c_0} e^{-z_0/z_1} + \frac{g}{c_0} (z - z_0), \end{aligned} \quad (9)$$

$c_0 = 1455$ m/s, $c_1 = 70$ m/s, $z_0 = 250$ m is the depth of the channel axis, i. e. the depth with the minimal sound speed, $z_1 = 30$ m, $g = 0.017$ s⁻¹. (see Fig. 1). The ocean bottom is assumed to be flat and placed at the depth $h = 3$ km. We consider only the deep-water propagation, albeit the source in the aforementioned experiments [27, 28] was mounted into the bottom in the coastal zone near the Gamov peninsula. The shallow-water part of the waveguide was relatively short, less than 30 km, and didn't have significant bottom features which could remarkably alter ray stability.

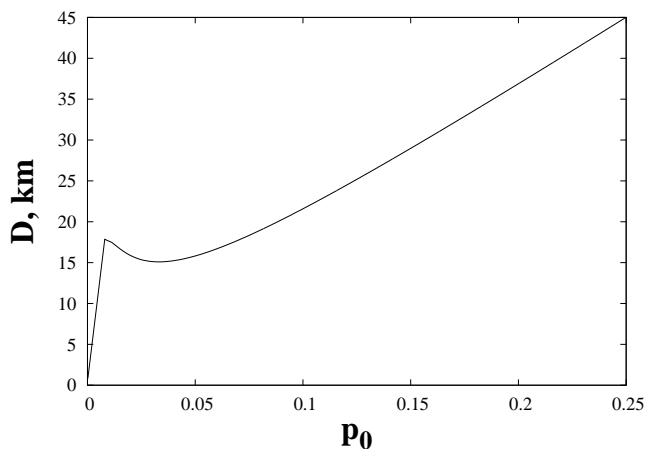


FIG. 2. Ray cycle length vs initial ray momentum for the source located at the channel axis.

Expressions (8) and (9) permit analytical derivation of the basic model characteristics in the absence of horizontal inhomogeneity. One can introduce the ray action

$$I = \frac{1}{\pi} \int_{z_{\min}}^{z_{\max}} \sqrt{2[E - U(z)]} dz, \quad (10)$$

where z_{\min} and z_{\max} are the upper and lower ray turning points, respectively, and $E = 0.5p^2 + U(z)$. Ray action describes steepness of a ray trajectory and enters into the Einstein-Brillouin-Keller quantization rule.

$$k_0 I_m = m - 1/2, \quad m = 1, 2, \dots \quad (11)$$

establishing the link between normal modes of the unperturbed waveguide and modal rays. Here I_m is the action of a modal ray, and both ray turning points are assumed to be inside the water column, that is, rays undergo total internal reflection due to smooth vertical gradient of the refractive index $n = c_0/c(z, r)$. Normal modes are the solutions of the Sturm-Liouville equation

$$-\frac{1}{2k_0^2} \frac{\partial^2 \phi_n(z)}{\partial z^2} + U(z) \phi_n(z) = E_n \phi_n(z), \quad (12)$$

with appropriate boundary conditions at the ocean surface and bottom. The main contribution to the mode m is given from the rays with $I \simeq I_m$ [9]. Integration of (10) yields

$$I = 2z_1 \sqrt{2E_{\min}} \left[\sqrt{\varepsilon} \ln(\sqrt{\varepsilon} + \sqrt{\varepsilon - 1}) - \sqrt{\varepsilon - 1} \right] + \frac{2\sqrt{2}c_0}{3g} (E - E_{\min})^{3/2}, \quad (13)$$

where $\varepsilon = E/E_{\min}$, $E_{\min} = (c_1/c_0) \exp(-z_0/z_1)$. Ray cycle length, i. e. horizontal distance between two successive upper (or lower) ray turning points, can be determined as

$$D(E) = 2\pi \frac{dI}{dE} = 2z_1 \sqrt{\frac{2}{E}} \ln(\sqrt{\varepsilon} + \sqrt{\varepsilon - 1}) + \frac{2c_0 \sqrt{2E_{\min}}}{g} \sqrt{\varepsilon - 1}. \quad (14)$$

Fig. 2 represents dependence of ray cycle length on initial ray momentum for the source located at the channel axis $z = 250$ m. Initial momentum p_0 depends on E as $p_0 = \sqrt{2(E - E_{\min})}$. Function $D(p_0)$ is nonmonotonic and has two extrema, the sharp maximum and the smooth minimum. The latter one can give rise to a so-called weakly-divergent beam [30–33]. Its low divergence is associated with approximate equality of cycle length values for rays forming the beam. It will be demonstrated in Section V that the local minimum of $D(p_0)$ plays a significant role in ray stability.

B. Sound-speed perturbation

Model of the internal-wave-induced sound-speed perturbation was built up in several steps. Firstly, we computed the range-averaged profile of buoyancy frequency, using the hydrological data [29]. Then, we calculated realizations of the sound-speed perturbation using the method proposed in [34]. In order to facilitate numerical simulation, the perturbation was expanded over empirical orthogonal functions [35]

$$\delta c(z, r) = \langle \delta c(z) \rangle + \sum_n b_n(r) Y_n(z). \quad (15)$$

Empirical orthogonal functions $Y_n(z)$ are the eigenvectors of the covariance matrix \hat{K} with elements

$$K_{ij} = \frac{1}{L} \sum_{l=1}^L [\delta c_l(z_i) - \langle \delta c(z_i) \rangle] [\delta c_l(z_j) - \langle \delta c(z_j) \rangle], \quad (16)$$

where index l numbers L statistically independent realizations of $\delta c(z)$, $\{z_i\}$ is a vector of depth values, and angular brackets mean ensemble average. As δc is caused by internal waves, one can set $\langle \delta c \rangle = 0$. Eigenvalues of the matrix \hat{K} quantify contributions from the corresponding

eigenvectors in the expansion (15). It was found that the contribution of the first orthogonal function prevails, and one can fairly represent the sound-speed perturbation as the product

$$V(z, r) = b_1(r) Y_1(z) \quad (17)$$

where $b_1(r)$ is a random function. For simplicity, it is assumed that $b_1(r)$ is a stochastic process with the exponentially-decaying autocorrelation function

$$\langle b_1(r) b_1(r') \rangle = \exp(-|r - r'|/\bar{r}), \quad (18)$$

where the correlation length \bar{r} is taken of 10 km, that is typical for the deep ocean [36]. Then the realizations of $b_1(r)$ can be computed via the formula $b_1 = \sqrt{2\bar{r}}\eta$, where η is a solution of the Ornstein-Uhlenbeck stochastic differential equation

$$\frac{d\eta}{dr} = -\frac{1}{\bar{r}}\eta(r) + \frac{1}{\bar{r}}\xi(r). \quad (19)$$

The procedure of solving this equation is described, for instance, in [37]. Here ξ is a Gaussian white noise satisfying

$$\langle \xi(r) \rangle = 0, \quad \langle \xi(r) \xi(r') \rangle = \delta(r - r'). \quad (20)$$

The resulting function $b_1(r)$ satisfies $\langle b_1^2(r) \rangle \simeq 1$.

The calculated function $Y_1(z)$ is depicted in Fig. 1(b). It involves step-like changes in the depth interval from 100 to 300 meters. These changes are caused by the depth discretization of the hydrological data and physically irrelevant. Wave modeling is insensitive to them, but ray-based calculations can be significantly affected. Therefore, in ray calculations we use a smooth analytical approximation

$$Y_1 = A y_a \exp(-y_a^n) + B \exp(-y_b^2), \quad (21)$$

where $A = 0.0027$, $y_a = z/z_a$, $n = 1.1$, $z_a = 24$ m, $B = 2 \cdot 10^{-5}$, $y_b = (z - z_c)/z_b$, $z_b = 50$ m, $z_c = 200$ m.

IV. FINITE-RANGE EVOLUTION OPERATOR

Finite-range evolution operator (FREO) had been introduced for studying wave propagation in a randomly-inhomogeneous waveguide in [14, 23]. Its quantum-mechanical analogue was earlier considered in [26]. Basically, a finite-range evolution operator (FREO) is an element of one-parameter group generated by the operator in the right-hand side of the equation (3). Consider a solution $\Phi(z, r)$ of the parabolic equation (3) complemented with the standard boundary conditions

$$\Phi|_{z=0} = 0, \quad \left. \frac{d\Phi}{dz} \right|_{z=h} = 0 \quad (22)$$

and the initial condition $\Phi(z, r=0) = \bar{\Phi}(z)$, where $\bar{\Phi}(z)$ belongs to $L^2[0, h]$ and satisfies (22). Then FREO $\hat{G}(\tau)$

is defined on the subspace of $L^2[0, h]$ (restricted by (22)) as

$$\hat{G}(\tau)\bar{\Phi}(z) \equiv \Phi(z, r)|_{r=\tau}. \quad (23)$$

By definition, the FREQ describes transformation of a wavefield in course of propagation along a finite waveguide segment of length τ . Each realization of inhomogeneity produces its own realization of the FREQ. Our interest is concerned with statistical properties of the FREQ and their connection to classical ray stability.

Note that the choice of the hard wall boundary condition at the bottom (22) is typical for the deep ocean acoustics problems when the attention is restricted to the trapped modes, whose propagation is not affected by the bottom interaction. Under these conditions no energy is absorbed by the bottom. Hence, if the attenuation in the sea water is negligible (this is true for the sound frequencies of our interest) and refraction index in (3) has no imaginary part, then the FREQ is a unitary operator.

FREQ can be represented as a matrix in the basis of normal modes $\phi_j(z)$ satisfying the Sturm-Liouville problem (12,22). Matrix elements of the FREQ are given by

$$G_{mn}(\tau) = \int_0^h \phi_m(z) \hat{G}(\tau) \phi_n(z) dz. \quad (24)$$

Thus, the matrix elements G_{mn} are complex-valued amplitudes of modal transitions. For the range-independent waveguide, the matrix of FREQ is diagonal with $|G_{mm}| = 1$.

Eigenvalues and eigenvectors of the FREQ obey the equation

$$\hat{G}\Psi_m(z, r) = g_m \Psi_m(z, r). \quad (25)$$

Owing to unitarity, eigenvalues g_m can be recast as

$$g_m = e^{-ik_0\epsilon_m}, \quad \epsilon_m \in \Re. \quad (26)$$

Since eigenvalues of the FREQ belong to the unit circle in the complex plane, the FREQ corresponds to the circular ensemble [25]. The FREQ has much in common with the Floquet operator governing wave propagation in a range-periodic waveguide [11, 12] and quantum dynamics in time-periodic systems. For instance, quantity ϵ_m is the analogue of quasienergy in quantum mechanics.

Note that eigenvalues of $\hat{G}(\tau)$ may be easily computed using its matrix representation $G_{mn}(\tau)$. To accomplish this one has to clip a finite block of this (infinite) matrix corresponding to the trapped modes, neglecting their interaction with high-order modes. This simplification is reasonable and does not affect accuracy of the eigenvalues computation (and the numerics confirms that) since the prevailing small-angle propagation corresponds to the low-order modes.

A. Level spacing statistics

Wave chaos reveals itself in the spectrum of the FREQ, in particular, in the statistics of level spacings. A level spacing is defined as

$$s = \frac{k_0 M (\epsilon_{m+1} - \epsilon_m)}{2\pi}, \quad m = 1, 2, \dots, M, \quad (27)$$

$$\epsilon_{M+1} = \epsilon_1 + \frac{2\pi}{k_0}.$$

where ϵ_m increases with increasing m , M is the total number of eigenvalues for a single realization of the FREQ, equal to the number of trapped modes.

Level spacing statistics can be studied in terms of the random matrix theory [25]. Regular dynamics implies that the matrix of the FREQ consists of separate independent blocks. Then level sequences contributed from different blocks are statistically independent, therefore, the resulting level spacing distribution obeys the Poisson law

$$\rho(s) \sim \exp(-s). \quad (28)$$

Under conditions of ergodic chaos, all normal modes are coupled to each other. This results in repulsion of neighbouring levels, the phenomenon closely related to spectral splittings induced by tunneling [38]. In this case level spacing statistics is described by the Wigner-Dyson distribution

$$\rho(s) \sim s^\zeta \exp(-Cs^2), \quad (29)$$

where constants ζ and C depend on symmetries of the FREQ. As the FREQ doesn't possess the symmetry $r \rightarrow -r$, it corresponds to the circular unitary ensemble (CUE) with $\zeta = 2$ and $C = 4/\pi$ [26].

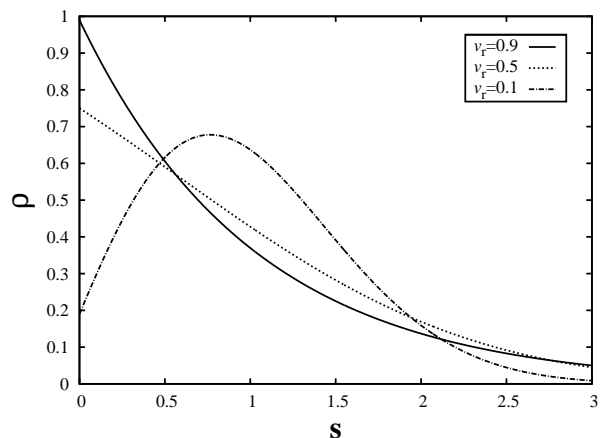


FIG. 3. Berry-Robnik distribution with $v_r = 0.9$, $v_r = 0.5$ and $v_r = 0.1$.

The most interesting case is mixed phase space, with the coexistence of regular and chaotic domains. Then

level spacing statistics should be described by some combination of Poisson and Wigner-Dyson laws. In the short-wavelength limit one can use the Berry-Robnik distribution [39]

$$\rho(s) = \left[v_r^2 \operatorname{erfc} \left(\frac{\sqrt{\pi}}{2} v_c s \right) + \left(2v_r v_c + \frac{\pi}{2} v_c^3 s \right) \exp \left(-\frac{\pi}{4} v_c^2 s^2 \right) \right] \exp(-v_r s), \quad (30)$$

where v_r and v_c are relative phase space volumes corresponding to regular and chaotic ray motion, respectively, $v_r + v_c = 1$. In (30), it is assumed that phase space consists of only two distinct domains: one regular and one chaotic.

Taking into account the correspondence between rays and modes established by the WKB representation (11), one can regard v_r as a fraction of modes whose refraction is regular, and v_c as a fraction of modes exhibiting wave chaos. In the limiting cases $v_r = 1$ and $v_c = 1$, Berry-Robnik formula (30) reduces to the Poisson distribution and the Wigner-Dyson distribution for the orthogonal ensemble ($\zeta = 1$), respectively. As is shown in Fig. 3, Berry-Robnik distribution undergoes smooth transition from the Poisson to the Wigner-Dyson law as v_r decreases from 1 to 0. Wigner-Dyson distributions for orthogonal ($\zeta = 1$) and unitary ($\zeta = 2$) ensembles are close to each other, therefore, one can use (30) as an approximation for the circular unitary ensemble. Berry-Robnik distribution is based on the assumption of the total statistical independence of the matrix blocks corresponding to regular and chaotic dynamics. This assumption is completely fulfilled only in the semiclassical limit. As wave corrections grow, independence degrades due to regular-to-chaotic tunneling [40]. Hence, Berry-Robnik formula cannot work perfectly for low-frequency sound propagation. In this case, a better fit is expected with the Brody distribution [41]

$$\rho(s) = (\beta + 1) A_\beta s^\beta \exp(-A_\beta s^{\beta+1}), \quad (31)$$

where $A_\beta = [\Gamma(\frac{\beta+2}{\beta+1})]^\beta$, Γ is the Euler gamma function. $\beta = 0$ corresponds to the Poisson distribution, $\beta = 1$ yields the Wigner-Dyson distribution with $\zeta = 1$. Unfortunately, the Brody distribution is semiempirical and doesn't have an explicit physical interpretation in the intermediate regime $0 < \beta < 1$.

Functions (30) and (31) should describe level spacing statistics for single realizations of the FREO. Very unfortunately, this is problematic because one encounters insufficiency of the statistical ensemble. Indeed, long-range sound propagation is feasible only with low acoustic frequencies of tens or hundreds Hz. In this frequency range, number of trapped modes doesn't exceed several hundreds. To resolve this problem, we consider ensemble-averaged level spacing distribution

$$\rho(s, \tau) = \lim_{N \rightarrow \infty} \frac{1}{N} \sum_{n=1}^N P_n(s, \tau), \quad (32)$$

where $P_n(s, \tau)$ is a level spacing distribution corresponding to n -th realization of FREO. Fitting the function $\rho(s, \tau)$ with the Berry-Robnik distribution (30), one can estimate number regularly propagating modes for various values of τ and, whereby, track the transition to chaos with increasing τ . However, it should be noted that formula (32) enables accurate estimate of v_r only if fluctuations of v_r are weak, otherwise one should take into account nonlinearity of ρ as a function of v_r in (30).

Likewise we can observe transformation of level spacing statistics by fitting (32) with the Brody distribution (31). Then the value of β corresponding to the best fit should increase with increasing τ from 0 to 1, reflecting wavefield stochasticization. Such calculations were performed in [14, 23] for a waveguide with a perturbed biexponential sound-speed profile.

B. Eigenfunction statistics

Wave chaos is also reflected in eigenfunction statistics of the FREO. Each eigenfunction can be expressed as a superposition of normal modes:

$$\Phi_m(z) = \sum_n c_{mn} \phi_n(z), \quad (33)$$

where c_{mn} is the m -th component of n -th eigenvector of the matrix \hat{G} , $\phi_n(z)$ is the n -th normal mode.

There are many methods for identification of "chaotic" eigenfunctions. In the present work we use only one of them. Ray chaos can lead to intense energy exchange between normal modes [9, 13, 24], therefore, a "chaotic" eigenfunction is a compound of many modes. The stronger chaos, the larger number of contributing modes. Hence, we can characterize "chaoticity" by estimating number of principal components [42] in the expansion (33). Number of principal components is calculated as

$$\nu(n) = \left(\sum_{m=1}^M |c_{mn}|^4 \right)^{-1}. \quad (34)$$

Number of principal components ν is equal to 1 in an unperturbed waveguide and grows as scattering intensifies, tending asymptotically to M .

V. ONE-STEP POINCARÉ MAP

In the geometrical acoustics approximation, dynamics of a wavepacket is represented as motion of some ray bundle. The bundle remains compact in course of propagation if ray dynamics is regular. Under conditions of ray chaos the bundle rapidly diverges. Initial conditions for rays contributing to the bundle can be found by means

of the Husimi function

$$W_h(p, z) = \left| \frac{1}{\sqrt[4]{2\pi\Delta_z^2}} \int dz' \Phi_0^*(z') \times \exp \left[ikp(z' - z) - \frac{(z' - z)}{4\Delta_z^2} \right] \right|^2, \quad (35)$$

projecting an initial wavepacket Φ_0 onto phase space of ray equations (7). In the limit $k_0 \rightarrow \infty$, the transformation (35) turns eigenfunctions Φ_m of the FREQ into some phase space sets which are invariant under the shift $r = 0 \rightarrow r = \tau$. The procedure proposed in [22] allows one to find out these sets in a randomly-inhomogeneous waveguide. This is the one-step Poincaré map (or the specific Poincaré map). The ray analogue of the map looks as follows:

$$p_{i+1} = p(r = \tau | p_i, z_i), \quad z_{i+1} = q(r = \tau | p_i, z_i), \quad (36)$$

where $p(r = \tau | p_i, z_i)$ and $z(r = \tau | p_i, z_i)$ are the solutions of ray equations (7) with initial conditions $p(r = 0) = p_i$, $z(r = 0) = z_i$. Values of p and z , calculated at the i -th step of mapping, become the initial conditions for the $(i + 1)$ -th step. This procedure is equivalent to the usual Poincaré map [18] for a range-periodic waveguide with the ray Hamiltonian

$$\bar{H} = \frac{p^2}{2} + U(z) + \tilde{V}(z, r). \quad (37)$$

Here $\tilde{V}(z, r)$ is periodic in r function

$$\tilde{V}(z, r' + n\tau) = V(z, r'), \quad 0 \leq r' \leq \tau, \quad (38)$$

where n is an integer. As it follows from (38), $\tilde{V}(z, r)$ is a sequence of identical pieces of $V(z, r)$, each of them has the length τ . Thus we replace the original randomly-perturbed Hamiltonian system by an equivalent periodically-perturbed one. This replacement is valid as long as we restrict ourselves by considering dynamics within the range interval $[0 : \tau]$. One-step Poincaré map can be considered as the classical counterpart of the FREQ.

Owing to analogy with the usual Poincaré map, the main property of the one-step Poincaré map can be formulated as follows: *each point of a continuous closed ray trajectory of the map (36) corresponds to a starting point of the solution of (7) which remains stable by Lyapunov till the range $r = \tau$.* The inverse statement is not, in general, true. Hence, the one-step Poincaré map provides a sufficient but not necessary criterion of stability.

Map (36) was studied in [3, 22, 43–45]. Here we shall give its brief description. It is reasonable to make canonical transformation of ray variables from momentum–depth $(p - z)$ to the action–angle (I, ϑ) . This procedure provides more appropriate representation of ray equations. The angle variable ϑ canonically conjugated to the action (10) is given by

$$\vartheta = \frac{\partial}{\partial I} \int_{z_0}^z p dz. \quad (39)$$

The transformed ray Hamiltonian is written as

$$\bar{H} = H_0(I) + \tilde{V}(I, \vartheta, r). \quad (40)$$

Ray equations in terms of the new variables:

$$\begin{aligned} \frac{dI}{dr} &= -\frac{\partial H}{\partial \vartheta} = -\frac{\partial V}{\partial \vartheta}, \\ \frac{d\vartheta}{dr} &= \frac{\partial H}{\partial I} = \omega(I) + \frac{\partial V}{\partial I}, \end{aligned} \quad (41)$$

where $\omega = 2\pi/D$ is spatial frequency of a ray trajectory in a waveguide. Perturbation $\tilde{V}(I, \vartheta)$ can be expanded into a double Fourier series

$$\tilde{V} = \frac{1}{2} \sum_{k, k'=1}^{\infty} V_{k, k'} e^{i(k\vartheta - k'\Omega r)} + \text{c. c.}, \quad (42)$$

where $\Omega = 2\pi/\tau$. Inserting (42) into (41), we obtain

$$\begin{aligned} \frac{dI}{dr} &= -\frac{i}{2} \sum_{k, k'=1}^{\infty} k V_{k, k'} e^{i(k\vartheta - k'\Omega r)} + \text{c. c.}, \\ \frac{d\vartheta}{dr} &= \omega + \frac{1}{2} \sum_{k, k'=1}^{\infty} \frac{\partial V_{k, k'}}{\partial I} e^{i(k\vartheta - k'\Omega r)} + \text{c. c.} \end{aligned} \quad (43)$$

If the condition

$$k'D(I) = k\tau \quad (44)$$

is fulfilled, there occurs resonance. The pair of integers k' and k determines multiplicity of resonance $k : k'$. Resonances occur at certain values of the action, which correspond to the so-called resonant torus. Ray dynamics in a small vicinity of a resonant torus with ray action I_0 can be described using the so-called resonance approximation [18], when one leaves only resonant terms in the r.h.s. of (43). It should be mentioned that one and the same resonant torus corresponds to an infinite number of resonances with multiplicities $(jk) : (jk')$, where j is an integer. However, resonance Fourier amplitudes $V_{k, k'}$ rapidly decrease with increasing k and k' , therefore, only few low-order resonances influence significantly ray dynamics. Consequently, we can take into account only some finite number of dominant resonances. For further simplification, we make the following procedures:

1. As \tilde{V} is a smooth function of z in the underwater sound channel considered, the derivative $d\tilde{V}/dI$ is small compared with ω , and the sum in the second equation of (43) can be dropped out.
2. Near resonance, spatial frequency ω can be expanded as $\omega = \Omega + \omega'_I \Delta I$, where $\omega'_I = d\omega/dI$.

Then introducing new variables

$$\Delta I = I - I_0, \quad \psi = k\vartheta - k'\Omega r, \quad (45)$$

and expressing $V_{k,k'}$ as $|V_{k,k'}| \exp(i\zeta_{k,k'})$, we can rewrite (43) as

$$\begin{aligned} \frac{d(\Delta I)}{dr} &= \sum_{l=1}^L lk|V_{lk,lk'}| \sin(l\psi + \zeta_{lk,lk'}) = -\frac{\partial \tilde{H}}{\partial \psi}, \\ \frac{d\psi}{dr} &= \omega_I \Delta I = \frac{\partial \tilde{H}}{\partial (\Delta I)}, \end{aligned} \quad (46)$$

where L is the number of dominant resonances, and

$$\tilde{H} = \omega_I' \frac{(\Delta I)^2}{2} + \sum_{l=1}^L lk|V_{lk,lk'}| \cos(l\psi + \zeta_{lk,lk'}). \quad (47)$$

If $L = 1$, (47) turns into the universal Hamiltonian of nonlinear resonance [3, 18], and a phase space portrait of Eqs. (46) contains the domain of finite motion enclosed by the separatrix and corresponding to trapping into resonance. Then maximal value ΔI on the separatrix is determined as

$$\Delta I_{\max} = 4\sqrt{\frac{k|V_{k,k'}|}{\omega_I'}} \quad (48)$$

The terms with $l > 1$ may deform the pendulum-like phase space portrait and, moreover, result in the presence of additional separatrices inside the domain of finite motion. The latter phenomenon can occur when the perturbation oscillates with depth [22].

Transition to global chaos in the one-step Poincaré map happens when neighbouring dominant resonances overlap. The criterion of overlapping is the well-known Chirikov criterion

$$\frac{\Delta I_{\max}}{\delta I} \geq 1. \quad (49)$$

Here δI is the distance between neighbouring dominant resonances in the action space. Its variability with τ for $\tau > D$ is described by equation

$$\delta I = \frac{2\pi}{\omega_I' \tau}, \quad (50)$$

that is, increasing of τ enhances resonance overlapping. Differences in phase space patterns corresponding to different realizations of the perturbation are associated with phase and amplitude fluctuations of Fourier-amplitudes $V_{k,k'}$. However, the contribution of these fluctuations is limited, therefore, the ratio of the phase space volumes corresponding to regular and chaotic motion is mainly controlled by τ and weakly varies from one realization to another (see below for an illustration). This property allows one to consider the one-step Poincaré map as an useful tool for studying randomly-driven dynamical systems of various physical origins.

Resonance approximation presented above fails under violation of the nondegeneracy condition $\omega_I' \neq 0$. In this case one should use more sophisticated approaches, one

of them is presented in [46]. We shall address this issue in the end of this Section.

Fig. 4 illustrates phase space portraits calculated using the one-step Poincaré map with three different realizations of the sound-speed perturbation. The jump of the derivative dU/dz at $z = z_0$ leads to fast growth of numerical error in ray calculations. Therefore, we replaced the expression (8) for $U(z)$ by the smoothed function

$$U(z) = U_1(z) + \frac{1}{2} \left[1 + \tanh \frac{z - z_0}{\Delta} \right] U_2(z), \quad (51)$$

where $\Delta = 1$ m. Each of the phase space portraits represents a mixed phase space structure consisted of regular and chaotic domains. Phase portraits with the same τ mainly differ only in angular locations of regular islands, whereas their overall structure is very similar. The main regular domain is placed near the point $z = z_0$, $p = 0$ and corresponds to flat rays intersecting the horizontal plane with the smallest angles. This circumstance deserves especial attention because stability of flat rays is not typical for sound propagation in the deep ocean. Numerous experiments on long-range sound propagation in the North-Eastern Pacific Ocean (see, for instance, [47–51]) indicate on strong irregularity of flat near-axial rays, associated with ray chaos [52, 53]. The “deterministic” mechanism of near-axial chaos is ray scattering on vertical resonances caused by small-scale depth oscillations of the sound-speed perturbation [12, 13, 15]. These oscillations are contributed from high-number modes of an internal-wave field. In the Sea of Japan, the effect of the high-number modes is weak, therefore, the sound-speed perturbation can be fairly described by equation (17), where depth dependence is given by a smooth function $Y_1(z)$. Weakness of high-number internal-wave modes is a peculiar feature of the Sea of Japan. It is caused by the specific form of the buoyancy frequency profile [28]. In particular, the waveguide for internal waves, determined by the buoyancy frequency profile, is too narrow. Consequently, it doesn’t efficiently focus high-number modes of low-frequency internal waves. As low-frequency internal waves give the dominant contribution into a total internal-wave field, depth oscillations of the perturbation are suppressed.

Resonance overlapping is enhancing as τ grows, and stable islands eventually submerge into the chaotic sea. However, there is a small region of stability that survives for distances of hundreds kilometers, transforming into a chain of islands around the region near $z = z_0$, $p = 0$. This chain corresponds to the smooth minimum of the function $D(p_0)$ depicted in Fig. 2. In the absence of inhomogeneity, this minimum gives rise to the so-called shearless torus in phase space, producing a weakly-divergent beam. It is recognized that shearless tori can possess extraordinary persistence to chaos [46, 54–57], therefore, a weakly-divergent beam can survive in the presence of a sound-speed perturbation. Hence, formation of a weakly-divergent beam can be considered as a possible mechanism responsible for unusual stability of near-axial rays,

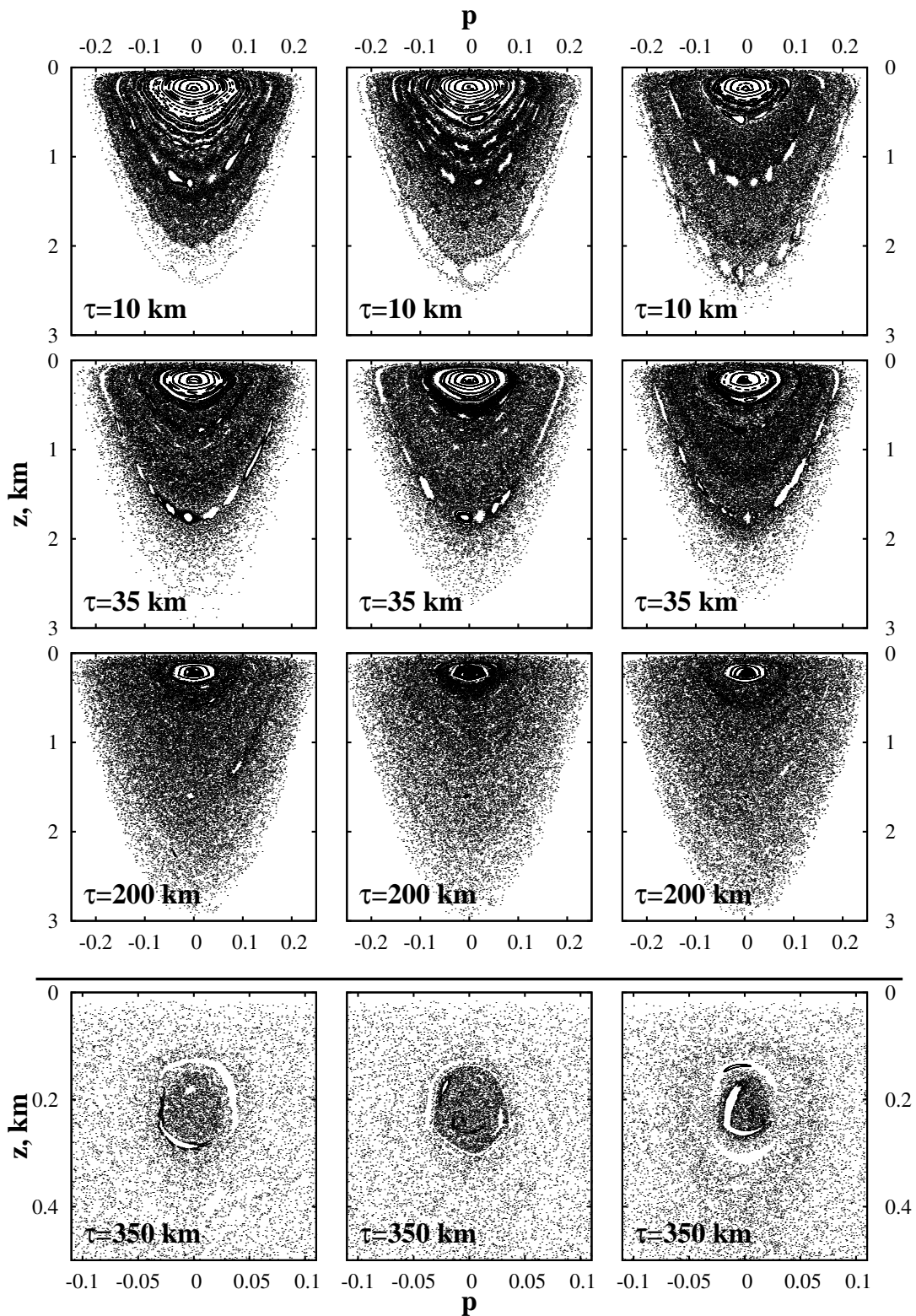


FIG. 4. Ray phase space portraits constructed via the one-step Poincaré map (36). Each column corresponds a single realization of the sound-speed perturbation. Value of τ is indicated in the left lower corner.

observed in experiments [27, 28].

VI. SPECTRAL STATISTICS OF FREO FOR THE UNDERWATER SOUND CHANNEL IN THE SEA OF JAPAN

A. General remarks

This section is devoted to numerical modeling of the FREO in the Sea of Japan. Each realization of the FREO

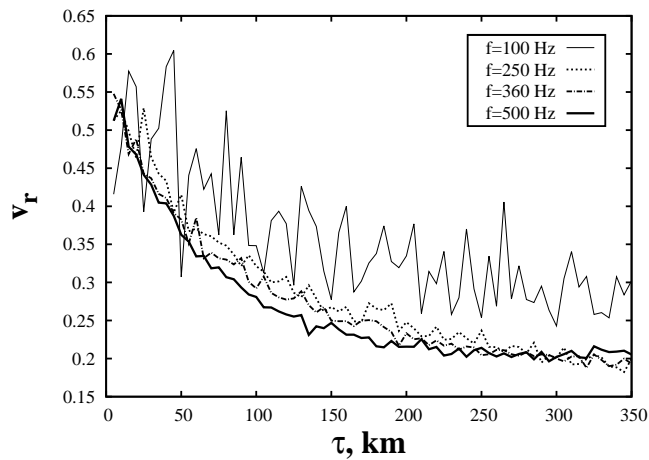


FIG. 5. Fraction of the phase space volume corresponding to regular motion vs distance τ for various frequencies.

was represented as a matrix in the basis of normal modes being solutions of the Sturm-Liouville problem (12) with the boundary conditions (22). Only purely-water modes which propagate without reaching the bottom were taken into account. They were selected using the criterion $E_m < U(z = h)$, where E_m is the m -th eigenvalue of the Sturm-Liouville problem (12). This criterion ensues from the WKB approximation for normal modes [9]. Number of trapped modes M depends on sound frequency. It is equal to 72 for $f = 100$ Hz, 179 for $f = 250$ Hz, 259 for $f = 360$ Hz, and 361 for $f = 500$ Hz. Statistical ensembles of the FREOs, corresponding to the frequencies of 250, 360 and 500 Hz, were calculated with 100 realizations of the perturbation. The ensemble corresponding to 100 Hz was calculated with 500 realizations. For each realization, we constructed a family of the FREOs $\hat{G}(\tau)$, where $\tau = 5, 10, 15, \dots, 350$ km.

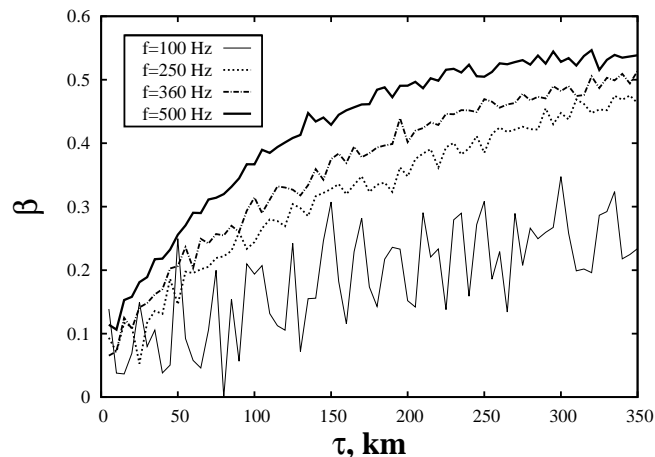


FIG. 6. The Brody parameter β vs distance τ .

B. Eigenvalue statistics

We calculated the ensemble-averaged level spacing distribution $\rho(s, \tau)$ using the formula (32) and fitted it, for each value of τ , by means of the Berry-Robnik (30) and Brody (31) distributions. Thus, we obtained dependencies of the regular phase space volume v_r and Brody parameter β on distance τ . As is shown in Fig. 5, v_r rapidly decreases in the first 100–150 km. Then, it becomes almost constant. This may indicate on the influence of the long-living stable islands in the vicinity of the weakly-divergent beam. Notably, the curves corresponding to 250, 360 and 500 Hz are very close to each other, whereas the curve corresponding to 100 Hz lies above them and undergoes strong fluctuations which persist even with increasing number of realizations. It should be mentioned that the above estimates of v_r have limited accuracy because the assumptions underlying the formula (30) are satisfied only approximately. Therefore, the results obtained using the Berry-Robnik distribution are rather qualitative than quantitative, especially for low sound frequencies.

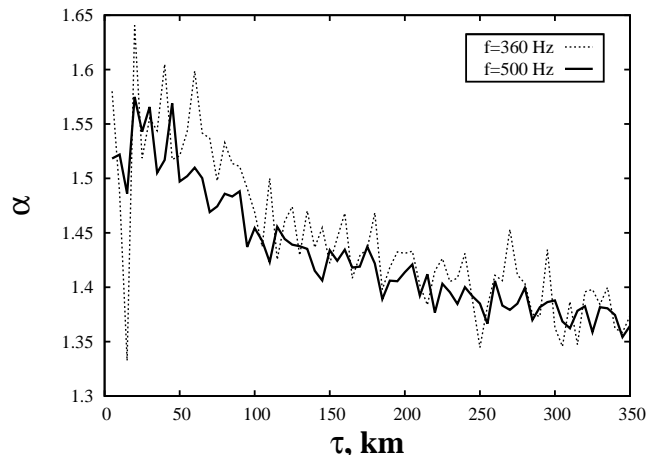


FIG. 7. Relano parameter α vs distance τ .

Approximation of level spacing statistics by means of the Brody distribution leads to qualitatively similar results. They are presented in Fig. 6. For frequencies 250, 360 and 500 Hz, the Brody parameter β gradually grows from 0 to 1, reflecting transformation from Poissonian to Wigner-like statistics. In the case of $f = 100$ Hz the growth is remarkably slower and affected by strong fluctuations. The fluctuations of v_r and β may be induced by regular-to-chaotic tunneling and dynamical localization, the phenomena whose influence on spectral statistics is still not well understood.

In addition, we used the method of spectral analysis, developed by A. Relano with coworkers in [58]. In this method, one firstly constructs a series

$$\delta_n = \sum_{i=1}^n (s_i - \langle s \rangle), \quad (52)$$

where $n = 1, 2, \dots, N-1$, N is the total number of eigenvalues. Then, making discrete Fourier transform

$$\bar{\delta}_k = \frac{1}{\sqrt{N}} \sum_n \delta_n \exp\left(\frac{2\pi i k n}{N}\right), \quad (53)$$

one finds the power spectrum

$$S(k) = |\bar{\delta}_k|^2. \quad (54)$$

Generally, ensemble-averaged spectrum obeys a power law

$$\langle S(k) \rangle \sim k^{-\alpha}. \quad (55)$$

Relano with coworkers found that regular dynamics corresponds to $\alpha = 2$, and global chaos results in $\alpha = 1$. In the mixed regime, α takes on an intermediate value between 1 and 2 [59]. Fig. 7 demonstrates that α decreases with increasing τ for the frequencies of 360 and 500 Hz, indicating gradual transition to chaos. However, α varies relatively slowly and remains near the middle value 1.5 for all distances considered, despite of the marked changes in the classical phase space portrait (see Fig. 4). Analogous dependencies for the frequencies of 100 and 250 Hz exhibit strong fluctuations and, therefore, are not presented in the figure. This implies that the method developed in [58, 59] provides good agreement only for relatively short wavelengths.

C. Eigenfunction analysis

Analysis of eigenfunctions possesses some advantages as compared with analysis of eigenvalues. The main advantage is the possibility to associate each eigenfunction with some set of normal modes and, whereby, associate it with a certain geometry of propagation. We can properly classify eigenfunctions, taking into account the interplay with normal modes. Such classification can be used for finding wavepacket configurations whose dynamics is expected to be less or more regular. Proper classification can be obtained using the parameter μ [11]. It is defined as

$$\mu = \sum_{m=1}^M |c_m|^2 m. \quad (56)$$

In an unperturbed waveguide, only one normal mode contributes to each eigenfunction, and μ coincides with the number of this mode. Taking into account the quantization rule (11), we obtain the formula

$$\langle I \rangle = \frac{\mu}{k_0} + \frac{1}{2k_0} \quad (57)$$

that gives mean action corresponding to an eigenfunction. According to (57), the parameter μ determines phase space location of the eigenfunction and can serve

as its identifier. Figures 8 and 9 illustrate eigenfunction distributions in the μ - ν plane, where ν is number of principal components (34), for the frequencies of 500 and 100 Hz, respectively.

Let us firstly consider Fig. 8 corresponding to the frequency of 500 Hz. Mode coupling is relatively weak for small values of τ , therefore, the distribution is mainly concentrated near $\nu = 1$. We want to focus attention on the dense spots elongated in the ν -direction. They correspond to eigenfunctions reflecting mode-medium resonance [9] being the wave counterpart of ray-medium resonance (44). Indeed, an isolated ray-medium resonance produces oscillations of ray action inside the interval $I_0 - \Delta I_{\max} \leq I \leq I_0 + \Delta I_{\max}$, where I_0 is a resonance action, ΔI_{\max} is resonance width in the action space. According to the principle of ray-mode duality, these oscillations of action correspond to coherent transitions between the normal modes whose numbers satisfy the inequality

$$m_0 - \Delta m \leq m \leq m_0 + \Delta m, \quad (58)$$

where $m_0 = k_0 I_0 + 1/2$, $\Delta m = k_0 \Delta I_{\max}$. Resonance-induced modal transitions give rise to eigenfunctions with $\mu \simeq m_0$ and ν varying from 1 to Δm . As long as resonance values of the action, being determined by τ , are the same for all realizations of the perturbation, these eigenfunctions form vertically-elongated concentrations of points in the μ - ν plane. Location of mode-medium resonances along the μ -axis can be found using the formula

$$k' D(I = \langle I \rangle) = k\tau, \quad (59)$$

where $\langle I \rangle$ is linked to μ by (57). Concentrations induced by mode-medium resonance disappear with increasing τ due to overlapping of mode-medium resonances and delocalization [60]. Delocalization leads to abrupt growth of number of principal components. It eventually subjects all eigenfunctions in the interval between $\mu \simeq 100$ and $\mu \simeq 300$, resulting in the “boomerang” pattern in the μ - ν plane, as illustrated in Fig. 8(d). Left and right ends of the “boomerang” are formed by weakly scattered eigenfunctions. The left end corresponds to the almost horizontal near-axial propagation, that is, its regularity can be associated with long-living stable islands in the one-step Poincaré map.

Eigenfunction distribution in the μ - ν plane for the frequency of 100 Hz possesses a more complicated structure. It is exceptionally regular for $\tau = 10$ km and $\tau = 35$ km, as shown in Figs. 9(a) and 9(b). Mode-medium resonances reveal themselves as “stalagmites”. Each stalagmite is drawn by a family of distinct weakly biased lines. Contours of the most pronounced stalagmite for $\tau = 35$ km are somewhat disordered and smeared. Some traces of stalagmite-like patterns survive even for distances of hundreds kilometers, despite of global overlapping of ray-medium resonances. Persistence of stalagmites for large τ indicates on the presence of eigenstates

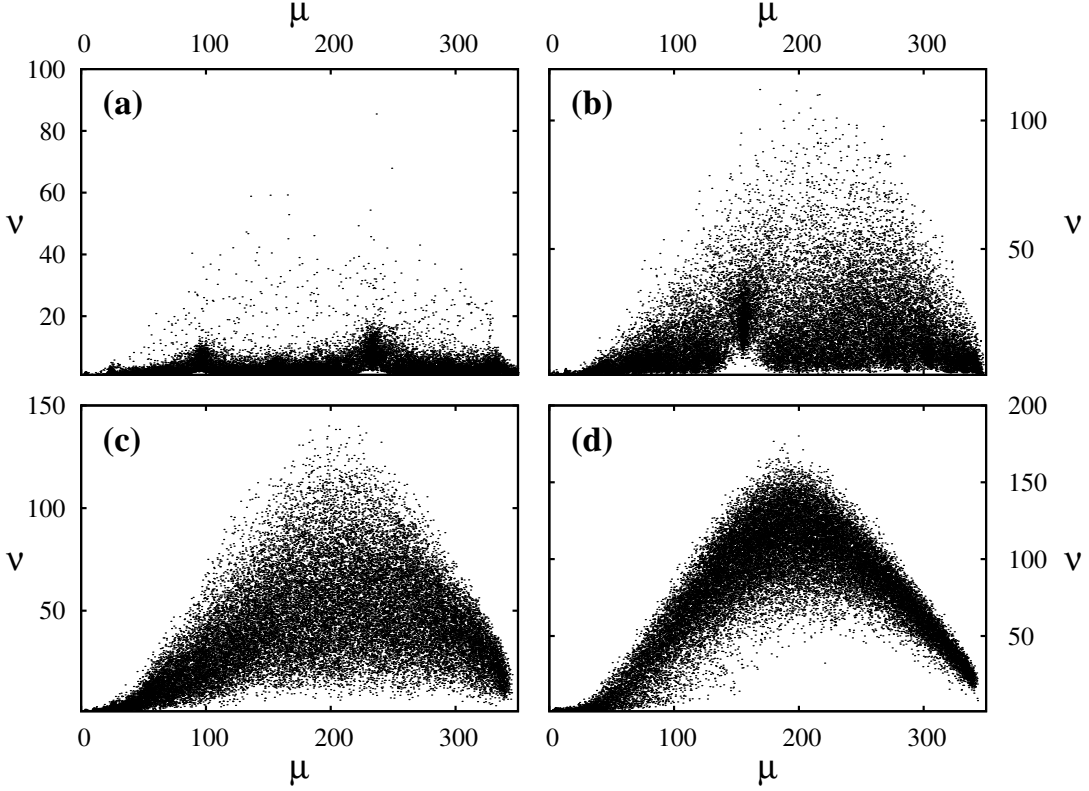


FIG. 8. Distribution of eigenfunctions in the μ - ν plane, where the parameter μ is given by (56), and ν is a number of principal components (34). Distance values: (a) $\tau = 10$ km, (b) $\tau = 35$ km, (c) $\tau = 100$ km, (d) $\tau = 350$ km. The sound frequency is 500 Hz.

localized near periodic orbits of the one-step Poincaré map. As long as these eigenstates correspond to non-spreading wavepackets, we can associate such localization with suppression of ray chaos and recovery of regular refraction in the vicinities of the periodic orbits. An analogous phenomenon had been reported in [12] for range-periodic waveguides.

Besides of stalagmites, Figs. 9(a) and 9(b) illustrate the patterns in the form of “bridges”. For instance, a pronounced “bridge” in the left part of Fig. 9(a) connects the points $\mu = 5$, $\nu = 1$ and $\mu = 30$, $\nu = 1$. The eigenfunctions producing the “bridges” are consisted of normal modes satisfying the condition

$$k_0(E_m - E_n) = \frac{2\pi l}{\tau}, \quad m > n. \quad (60)$$

The aforementioned “bridge” in the Fig. 9(a) satisfies (60) with $m = 30$, $n = 5$, and $l = 9$. Condition (60) is equivalent to quantum resonance between two energy levels. In the ray limit

$$k_0(E_m - E_n) \rightarrow (m - n) \frac{dE}{dI} \equiv \frac{2\pi(m - n)}{D}, \quad (61)$$

and condition (60) reduces to (44). Each realization of the FREQO can yield eigenfunctions manifesting resonance (60). If resonance (60) corresponding to some

numbers (l, m, n) is localized, i. e. the modes m and n are not affected by other resonances, then the respective eigenfunction is a superposition of normal modes m and n ,

$$\Phi_{\text{res}}(z) \simeq c_m \phi_m + c_n \phi_n, \quad |c_m|^2 + |c_n|^2 \simeq 1. \quad (62)$$

As this takes place, the ratio of amplitudes $|c_m|/|c_n|$ is determined by the phase of the resonance harmonics of the perturbation. For the perturbation (17), amplitude of the l -th resonance harmonics reads

$$B_l = \frac{1}{2\pi} \int_0^{2\pi/\tau} b_1(r) \exp\left(-i \frac{2\pi l r}{\tau}\right) dr. \quad (63)$$

Phase of the resonance harmonics is a random quantity with uniform probability density in the range $[0 : 2\pi]$. Each value of the phase uniquely determines the values of μ and ν via the formulae

$$\mu = |c_m|^2 m + |c_n|^2 n, \quad (64)$$

$$\nu = (|c_m|^4 + |c_n|^4)^{-1}. \quad (65)$$

It turns out that quantities μ and ν are correlated for each eigenfunction corresponding to localized resonance

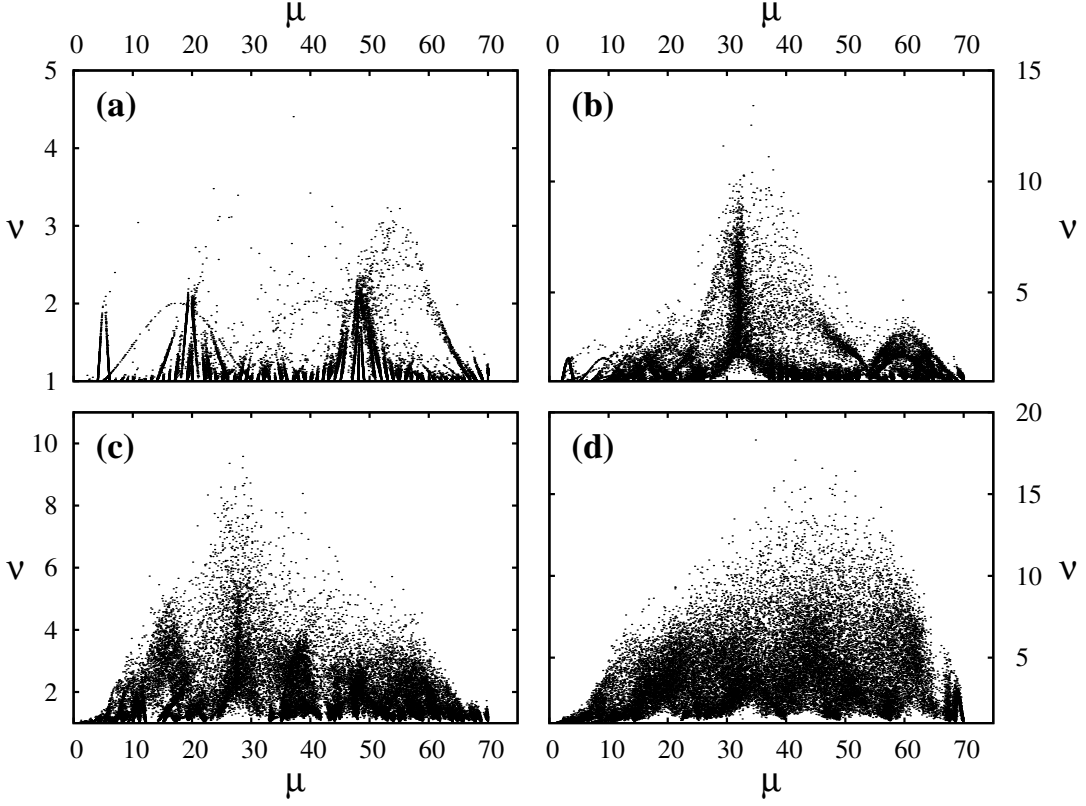


FIG. 9. The same as in Fig. 8, but for the frequency of 100 Hz. (a) $\tau = 10$ km, (b) $\tau = 35$ km, (c) $\tau = 100$ km, (d) $\tau = 350$ km.

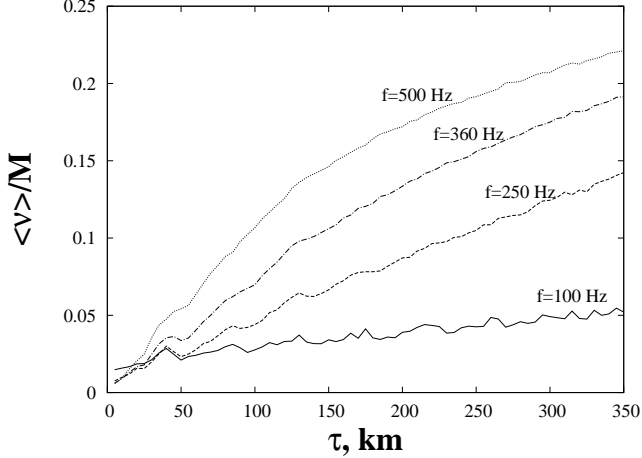


FIG. 10. Mean number of principal components as function of distance.

(60). This results in formation of “bridges” in the μ - ν plane. Localization becomes violated with increasing τ , therefore, correlation between ν and μ ceases, and ordered “bridges” transform into disordered clouds of points.

The above analysis shows that there are qualitative dif-

ferences in sound scattering for different frequencies. To estimate these differences quantitatively, we need a suitable parameter characterizing scattering strength. For example, chaos-induced phase space delocalization can be measured by the ensemble-averaged number of principal components, divided by the total number of trapped modes. As it follows from Fig. 10, the rate of delocalization increases with increasing sound frequency. This implies that chaotic diffusion associated with ray chaos degrades with increasing sound wavelength. It can be thought of as a manifestation of dynamical localization [25], an analogue of Anderson localization, when destructive interference suppresses wavepacket spreading.

In practice, it is useful to know fraction of the eigenfunction ensemble corresponding to regular propagation. This quantity can be regarded as an analogue of the parameter ν_r in the Berry-Robnik distribution. It can be estimated by means of the cumulative distribution function

$$F(\nu) = \int_1^{\nu} \rho(\nu') d\nu', \quad (66)$$

where $\rho(\nu')$ is the probability density function of ν . We can conditionally distinguish two regimes of localization: strong localization and moderate localization. Strong localization implies that eigenfunction of FREQ is close to

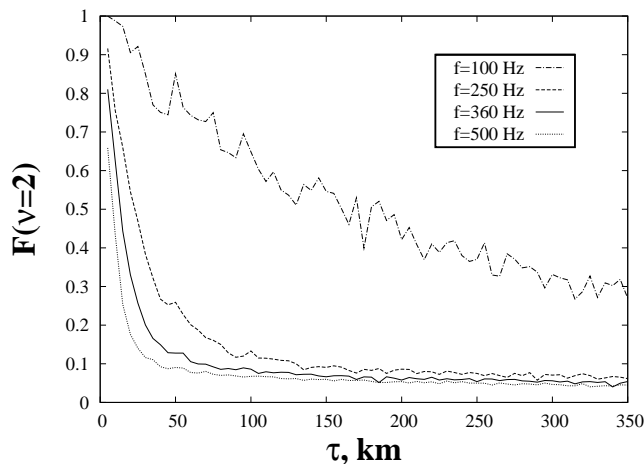


FIG. 11. Fraction of strongly-localized eigenfunctions as function of distance. The criterion of strong localization is the inequality $\nu \leq 2$.

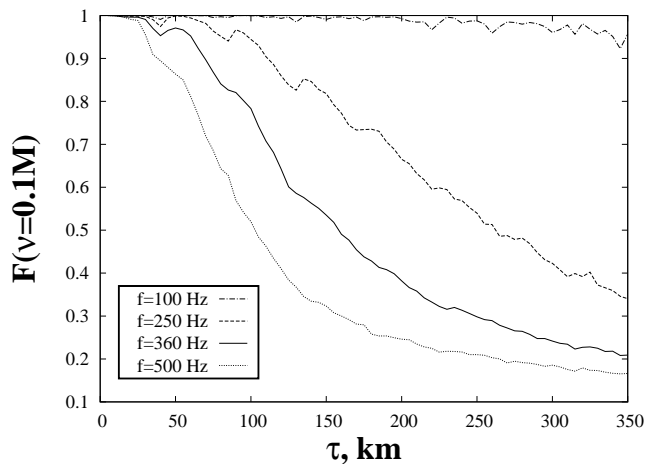


FIG. 12. Fraction of moderately localized eigenfunctions vs distance. The criterion of moderate localization is the inequality $\nu \leq 0.1M$, where M is the number of trapped modes.

one of normal modes of the unperturbed waveguide. To select strongly-localized eigenfunctions, we can use the inequality $\nu \leq 2$. Dependence of $F(2)$ on the horizontal distance τ is depicted in Fig. 11. Evidently, fraction of strongly-localized eigenfunctions is much larger for $f = 100$ Hz than for higher frequencies. The curves corresponding to the higher frequencies are close to each other. They drop down in the range of small τ , then decreasing of $F(2)$ becomes very slow. Slow decreasing can be linked to the presence of the long-living islands in the neighbourhood of the weakly-divergent beam.

In the regime of moderate localization, mode coupling can be sufficiently strong, but an eigenfunction occupies relatively small phase space volume, that is, number of

principal components is limited. We use the inequality $\nu \leq 0.1M$ as the criterion of moderate localization. As is demonstrated in Fig. 12, almost all eigenfunctions corresponding to the frequency of 100 Hz are moderately-localized. This is not the case of higher frequencies, when fraction of moderately-localized eigenfunctions significantly decreases with τ . We can conclude that decreasing of sound frequency can result in remarkable suppression of wavepacket diffusion in phase space.

VII. CONCLUSION

Spectral analysis of the finite-range evolution operator prompts a way to explore wave dynamics in a randomly-inhomogeneous waveguide by means of the quasideterministic approach, involving resonances, periodic orbits, phase space portraits, e.t.c. This approach was originally proposed in [14, 23]. The present work is devoted to its further development. We demonstrate various methods of spectral analysis. For instance, fitting of level spacing statistics by means of the Berry-Robnik distribution yields approximate estimate for fraction of regularly propagating normal modes of a waveguide. Also we use the method developed by A. Relano with coworkers, and consider distribution of eigenfunctions in the μ - ν space. In our opinion, the latter approach is the most robust, albeit its analytical description is lacking. The most important advantage of the eigenfunction analysis is the possibility to study separately scattering of different modes of a waveguide and find out the modes corresponding to regular propagation. A detailed view of the eigenfunction distribution in the μ - ν space suggests that the mechanism of the chaos onset with increasing distance can be associated with overlapping and delocalization of mode-medium resonances. The approach based on the statistical analysis of level spacings by means of the Berry-Robnik formula gives qualitative description of the transition but doesn't ensure quantitative agreement. The Relano method and the method based on the Brody distribution also give the qualitative description but cannot make any quantitative estimates due to their semiempirical nature.

We consider the underwater sound channel in the Sea of Japan as an example. Our analysis shows that almost horizontal near-axial sound propagation preserves regularity over distances of hundreds kilometers. There are two factors responsible for near-axial stability. The first factor is the peculiar hydrological structure in the region considered, resulting in the absence of vertical oscillations of the sound-speed perturbation. This circumstance leads to a qualitatively different scenario of ray chaos, as compared with the well-known acoustic experiments in the North-Eastern Pacific Ocean. The second factor is the formation of the weakly-divergent beam supported by long-living stable islands in classical phase space. Weakly-divergent beam occurs in the vicinity of the shearless torus. Non-dispersive motion of quantum

wavepackets near shearless tori was earlier observed in [61]. Also, we should emphasize that sound propagation with the frequency of 100 Hz reveals exceptionally high degree of stability, indicating on different physics of scattering for low sound frequencies. This phenomenon can be associated with strong dynamical localization.

We suppose that applicability of the approach presented in this paper is not limited to the problems of wave propagation in random media. An analogue of the FREQO can be readily used for studying of noise-induced quantum transport and related phenomena. We suggest that

combination of deterministic and statistical approaches should provide an insightful view on details of dynamics, especially in the presence of intermittency or synchronization.

This work was supported by the Russian Foundation of Basic Research (projects 09-05-98608 and 09-02-01258-a), the Federal Program “World Ocean” and the “Dynasty” Foundation. Authors are grateful to A.R. Kolovsky, S. Tomsovic, O.A. Godin, K.V. Koshel and V.V. Novotryasov for helpful comments concerning the subject of the research.

-
- [1] R. C. Shockley, J. Northrop, P. G. Hansen, and C. Hartdegen, *J. Acoust. Soc. Am.* **71**, 51 (1982).
- [2] W. H. Munk, W. C. O'Reilly, and J. L. Reid, *J. Phys. Oceanography* **18**, 1876 (1988).
- [3] D. Makarov, S. Prants, A. Virovlyansky, and G. Zaslavsky, *Ray and wave chaos in ocean acoustics: chaos in waveguides*, Series on complexity, nonlinearity and chaos (World Scientific, Singapore, 2009) p. 388.
- [4] K. B. Smith, M. G. Brown, and F. D. Tappert, *J. Acoust. Soc. Am.* **91**, 1939 (1992).
- [5] I. P. Smirnov, A. L. Virovlyansky, and G. M. Zaslavsky, *Phys. Rev. E* **64**, 036221 (2001).
- [6] M. G. Brown, J. A. Colosi, S. Tomsovic, A. L. Virovlyansky, M. A. Wolfson, and G. M. Zaslavsky, *J. Acoust. Soc. Am.* **113**, 2533 (2003).
- [7] D. V. Makarov, M. Y. Uleysky, and S. V. Prants, *Chaos* **14**, 79 (2004).
- [8] F. J. Beron-Vera and M. G. Brown, *J. Acoust. Soc. Am.* **115**, 1068 (2004).
- [9] A. L. Virovlyansky and G. M. Zaslavsky, *Phys. Rev. E* **59**, 1656 (1999).
- [10] I. P. Smirnov, A. L. Virovlyansky, and G. M. Zaslavsky, *Chaos* **14**, 317 (2004).
- [11] I. P. Smirnov, A. L. Virovlyansky, M. Edelman, and G. M. Zaslavsky, *Phys. Rev. E* **72**, 026206 (2005).
- [12] L. E. Kon'kov, D. V. Makarov, E. V. Sosedko, and M. Y. Uleysky, *Phys. Rev. E* **76**, 056212 (2007).
- [13] D. V. Makarov, L. E. Kon'kov, and M. Y. Uleysky, *Acoust. Phys.* **54**, 382 (2008).
- [14] A. L. Virovlyansky, D. V. Makarov, and S. V. Prants, *Phys. Usp.* **55** (2012).
- [15] K. C. Hegewisch, N. R. Cerruti, and S. Tomsovic, *J. Acoust. Soc. Am.* **117**, 1582 (2005).
- [16] W. Munk and C. Wunsch, *Deep Sea Res. Part A.* **26**, 123 (1979).
- [17] F. D. Tappert and X. Tang, *J. Acoust. Soc. Am.* **99**, 185 (1996).
- [18] G. M. Zaslavsky, *The physics of chaos in Hamiltonian systems* (Imperial College Press, London, 2007) p. 328.
- [19] L. B. Dozier and F. D. Tappert, *J. Acoust. Soc. Am.* **63**, 353 (1978).
- [20] J. A. Colosi and A. K. Morozov, *J. Acoust. Soc. Am.* **126**, 1026 (2009).
- [21] M. A. Wolfson and S. Tomsovic, *J. Acoust. Soc. Am.* **109**, 2693 (2001).
- [22] D. V. Makarov, M. Y. Uleysky, M. V. Budyansky, and S. V. Prants, *Phys. Rev. E* **73**, 066210 (2006).
- [23] D. V. Makarov, L. E. Kon'kov, and M. Y. Uleysky, ArXiv e-prints (2010), arXiv:1008.3037 [nlin.CD].
- [24] K. C. Hegewisch and S. Tomsovic, *Europhys. Lett.* **97**, 34002 (2012).
- [25] H. J. Stöckmann, *Quantum Chaos: An Introduction* (Cambridge University Press, Cambridge, 2007) p. 384.
- [26] A. R. Kolovsky, *Phys. Rev. E* **56**, 2261 (1997).
- [27] V. Bezotvetnykh, A. Burenin, Y. Morgunov, and Y. Polovinka, *Acoust. Phys.* **55**, 376 (2009).
- [28] R. C. Spindel, J. Na, P. H. Dahl, S. Oh, C. Eggen, Y. G. Kim, V. A. Akulichev, and Y. N. Morgunov, *IEEE J. Ocean. Engin.* **28**, 297 (2003).
- [29] “Oceanography and marine environment of the Far Eastern Region of Russia (proj. leader Rostov I. D.),” <http://www.pacificinfo.ru/en>.
- [30] L. M. Brekhovskikh, V. V. Goncharov, S. A. Dremuchev, V. M. Kurteпов, V. G. Selivanov, and Y. A. Chepurin, *Sov. Phys. Acoust.* **36**, 461 (1990).
- [31] I. Smirnov, J. Caruthers, and A. Khil'ko, *Radiophys. Quantum Electron.* **42**, 864 (1999).
- [32] A. K. Morozov and J. A. Colosi, *J. Acoust. Soc. Am.* **117**, 1611 (2005).
- [33] Y. Petukhov, *Acoust. Phys.* **55**, 785 (2009).
- [34] J. A. Colosi and M. G. Brown, *J. Acoust. Soc. Am.* **103**, 2232 (1998).
- [35] L. R. LeBlanc and F. H. Middleton, *J. Acoust. Soc. Am.* **67**, 2055 (1980).
- [36] L. B. Dozier and F. D. Tappert, *J. Acoust. Soc. Am.* **64**, 533 (1978).
- [37] K. Mallick and P. Marcq, *Phys. Rev. E* **66**, 041113 (2002).
- [38] L. D. Landau and E. M. Lifshitz, *Course of theoretical physics.*, Vol. 3: Quantum mechanics. Nonrelativistic theory (Pergamon Press, Oxford, 1977).
- [39] M. V. Berry and M. Robnik, *J. Phys. A: Math. Gen.* **17**, 2413 (1984).
- [40] A. Bäcker, R. Ketzmerick, and A. G. Monastra, *Phys. Rev. Lett.* **94**, 054102 (2005).
- [41] T. Prosen and M. Robnik, *J. Phys. A: Math. Gen.* **27**, 8059 (1994).
- [42] I. Varga and J. Pipek, *Phys. Rev. E* **68**, 026202 (2003).
- [43] D. Makarov and M. Uleysky, *J. Phys. A: Math. Gen.* **39**, 489 (2006).
- [44] C. Gan, Q. Wang, and M. Perc, *J. Physics A: Math. Theor.* **43**, 125102 (2010).
- [45] C. Gan and H. Lei, *J. Sound Vib.* **330**, 2174 (2011).
- [46] I. I. Rypina, M. G. Brown, F. J. Beron-Vera,

- H. Koçak, M. J. Olascoaga, and I. A. Udovydchenkov, *Phys. Rev. Lett.* **98**, 104102 (2007).
- [47] J. L. Spiesberger and F. D. Tappert, *J. Acoust. Soc. Am.* **99**, 173 (1996).
- [48] P. F. Worcester, B. D. Cornuelle, J. A. Hildebrand, J. William S. Hodgkiss, T. F. Duda, J. Boyd, B. M. Howe, J. A. Mercer, and R. C. Spindel, *J. Acoust. Soc. Am.* **95**, 3118 (1994).
- [49] P. F. Worcester, B. D. Cornuelle, M. A. Dzieciuch, W. H. Munk, B. M. Howe, J. A. Mercer, R. C. Spindel, J. A. Colosi, K. Metzger, T. G. Birdsall, and A. B. Baggeroer, *J. Acoust. Soc. Am.* **105**, 3185 (1999).
- [50] K. E. Wage, M. A. Dzieciuch, P. F. Worcester, B. M. Howe, and J. A. Mercer, *J. Acoust. Soc. Am.* **117**, 1565 (2005).
- [51] N. S. Grigorieva, G. M. Fridman, J. A. Mercer, R. K. Andrew, M. A. Wolfson, B. M. Howe, and J. A. Colosi, *J. Acoust. Soc. Am.* **125**, 1919 (2009).
- [52] J. Simmen, S. M. Flatte, and G.-Y. Wang, *J. Acoust. Soc. Am.* **102**, 239 (1997).
- [53] F. J. Beron-Vera, M. G. Brown, J. A. Colosi, S. Tomsovic, A. L. Virovlyansky, M. A. Wolfson, and G. M. Zaslavsky, *J. Acoust. Soc. Am.* **114**, 1226 (2003).
- [54] D. del Castillo-Negrete, J. M. Greene, and P. J. Morrison, *Physica D* **91**, 1 (1996).
- [55] M. V. Budyansky, M. Y. Uleysky, and S. V. Prants, *Phys. Rev. E* **79**, 056215 (2009).
- [56] M. Y. Uleysky, M. V. Budyansky, and S. V. Prants, *Phys. Rev. E* **81**, 017202 (2010).
- [57] M. Uleysky, M. Budyansky, and S. Prants, *J. of Exp. and Theor. Phys.* **111**, 1039 (2010).
- [58] A. Relaño, J. M. G. Gómez, R. A. Molina, J. Retamosa, and E. Faleiro, *Phys. Rev. Lett.* **89**, 244102 (2002).
- [59] A. Relaño, *Phys. Rev. Lett.* **100**, 224101 (2008).
- [60] G. P. Berman and A. R. Kolovskii, *Sov. Phys. Usp.* **35**, 303 (1992).
- [61] K. Kudo and T. S. Monteiro, *Phys. Rev. E* **77**, 055203 (2008).